Microsyst Technol (2012) 18:1615–1622
DOI 10.1007/s00542-012-1599-5

TECHNICAL PAPER

Design of suspension-based and collocated dual stage actuated suspensions

David Lengert · Edmund B. Fanslau Jr. · Frank E. Talke

Received: 30 September 2011 / Accepted: 13 June 2012 / Published online: 3 July 2012

Abstract Dual stage actuators have recently been implemented in hard disk drive suspensions in order to increase the track density of hard disk drives. This paper investigates the lateral deflection (lateral stroke), stress distribution and design characteristics of a suspension-based and a collocated flexure-based dual stage actuated suspension design using finite element analysis. Design parameters for each suspension design are examined and guidelines for improved lateral deflection characteristics are proposed.

1 Introduction

In order to increase the track density in magnetic recording disk drives, off-track motion between the read–write head and a written track must be minimized. One of the largest contributors to off-track motion is the sway-mode of a suspension. The sway mode frequency of a typical suspension has increased from approximately 5–10 kHz (Kilian et al. 2003) a decade ago to frequencies on the order of 20–30 kHz in present day suspensions. A number of dual stage actuated suspensions (DSAs) has been presented and discussed in recent years (Lau and Du 2005; Kim and Lee 2004; Evans and Griesbach 1999; Koganezawa et al. 1998; Mori et al. 1991). DSAs can be classified into "suspension-based" and "collocated" dual stage designs. In a suspension-based design, piezoelectric elements (PZTs) are mounted at the base of the suspension while in a collocated design one or more PZTs are located close to the head, ideally "collocated" with the head.

The principle of a typical suspension-based DSA is that a radial motion of the read–write head is achieved if a voltage is applied to the PZTs mounted at the base of the suspension. This motion is used for accurately positioning the read–write head on the desired track (Devasia et al. 2007). For suspension-based DSAs, the magnitude of the radial motion of the head is a function of the distance between the position of the PZTs at the base of the suspension and the position of the read–write element (Zhong and Sun 2004). Although a large distance is desirable from the point of view of achieving a large lateral displacement (stroke) of the head, a large distance reduces the accuracy and frequency response of suspension-based DSAs. A location of the PZTs very close to the head, as in collocated DSAs, is much more desirable from the point of view of frequency response and accuracy of head positioning. However, the reduced stroke of collocated DSAs and the efficiency of converting the PZT voltage into sufficiently large lateral displacements are important design considerations not yet fully understood for collocated DSAs. Typical DSAs have two PZTs arranged in a "push–pull" mode at the base of the suspension. If energized, one of the PZTs expands while the other one contracts.

In addition to a typical push–pull arrangement, Lau and Du (2006) proposed a piezoelectric quad-morph actuated suspension with advanced mechanical characteristics.

D. Lengert · F. E. Talke
Center for Magnetic Recording Research,
University of California, 9500 Gilman Drive, La Jolla,
San Diego, CA 92093-0401, USA
e-mail: ftalke@ucsd.edu

D. Lengert (✉)
University of Rostock, Albert-Einstein-Str. 2,
18059 Rostock, Germany
e-mail: david.lengert@gmail.com

E. B. Fanslau Jr.
JDS Uniphase Corporation, N. McCarthy Blvd.,
Milpitas, CA 95035, USA
e-mail: edmund.fanslau@jdsu.com

In this paper, a finite element investigation of a typical suspension-based DSA and a typical flexure-based collocated DSA is undertaken to determine the displacement characteristics of each type of suspension. Guidelines for the design and optimization of both types of suspensions in terms of achievable stroke are presented. For each design, the distance between (swage) hole and dimple was kept constant (11 mm). The dimple is defined as the pivot point between slider and suspension load beam.

2 Suspension-based DSA design

In Fig. 1 the design of a suspension-based DSA is shown, consisting of the so-called base, two PZTs, the load beam and the flexure. Typical dimensions for this design are indicated in the table below Fig. 1. The PZTs are glued to both the base and the load beam using non-conductive adhesive.

If a voltage is applied to the oppositely polarized PZTs, one PZT contracts while the other expands. This causes a lateral displacement (lateral stroke) of the read–write head as shown schematically in Fig. 2 (dashed lines).

To achieve the largest displacement for a given input voltage the design of a DSA suspension must be optimized. For a base-actuated DSA suspension, the parameters of greatest interest in the optimization of performance are (Fig. 3).

- width w_{bridge} of the center piece (bridge) between PZTs (Fig. 3a, b),
- distance w_{PZT} between PZTs (Fig. 3a, b),
- width of the gap $\Delta d = (w_{PZT} - w_{bridge})/2$ between PZT and base center piece (Fig. 3b), with $w_{PZT} > w_{bridge}$.

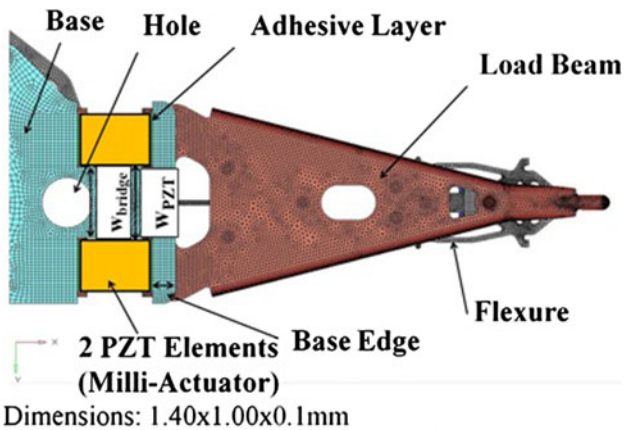

Dimensions: 1.40x1.00x0.1mm

Distance PZTs w_{PZT} (mm)	1.50
Bridge width w_{bridge} (mm)	1.40
Edge width w_{edge} (mm)	0.45
Thickness adhesive t_{adh} (mm)	0.05

Fig. 1 *Top view* of suspension-based DSA design with typical dimensions

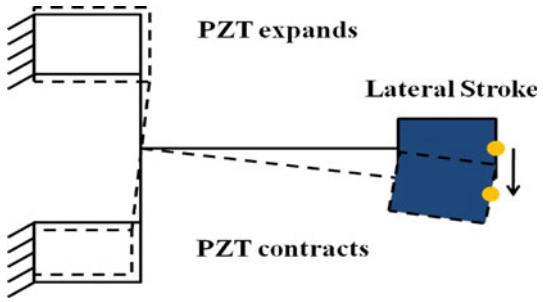

Fig. 2 Operating principle of suspension-based DSA design

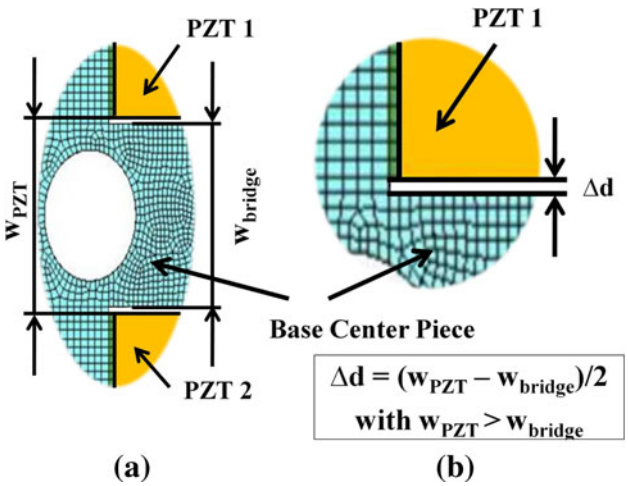

Fig. 3 Design parameters of suspension-based actuator for **a** distance between PZTs w_{PZT} and width of base center piece (*bridge*) w_{bridge} and **b** width of gap Δd

LS DYNA and HyperMesh, two commercially available software programs, were used to perform a thermo-structural analysis of the suspension-based DSA design shown in Fig. 1. Instead of applying a current or voltage, a thermal load, in terms of temperature T, was chosen to deform the PZTs and to simulate the piezoelectric effect. The orthotropic coefficient of thermal expansion was matched to the corresponding piezoelectric constants d_{zx} (=d_{zy}) and d_{zz}. At finite points of the PZT the deformation caused by the piezoelectric effect was numerically calculated using the piezoelectric material constants shown in Table 1. Then, with the help of comparative and convergence studies, the coefficient of thermal expansion was correlated to the piezoelectric constants of the PZT. The relationship between initial and deformed shape of a PZT can be expressed along the three coordinate axes as

$$\Delta l = d_{31} \times V \times \frac{l}{t}, \quad (1)$$

$$\Delta w = d_{31} \times V \times \frac{w}{t}, \quad (2)$$

Table 1 Material properties of piezoelectric element

Piezoelectric constant	
d_{31}	7.30×10^{-10} (m/V)
d_{33}	-3.30×10^{-10} (m/V)
d_{15}	7.80×10^{-10} (m/V)
Elastic compliance	
$S_{11} = S_{22}$	1.67×10^{-11} (m s^2/kg)
S_{33}	2.16×10^{-11} (m s^2/kg)
$S_{44} = S_{55}$	4.04×10^{-11} (m s^2/kg)
S_{66}	4.38×10^{-11} (m s^2/kg)
S_{12}	-5.18×10^{-11} (m s^2/kg)
$S_{13} = S_{23}$	-1.04×10^{-11} (m s^2/kg)

$$\Delta t = d_{33} \times V \times \frac{t}{t} = d_{33} \times V, \tag{3}$$

where Δl, Δw, and Δt denote the change of length l, width w, and thickness t, respectively, while "d_{31}" and "d_{33}" denote the piezoelectric constants of the PZT elements.

The PZTs, the slider and the E-block were modeled using constant strain solid finite elements with eight nodes and three degrees of freedom at each node. The suspension including flexure and load beam were simulated with constant thickness shell elements with three or four nodes and six degrees of freedom at each node.

3 Finite element simulation results for suspension-based DSA design

Comparing the resonance frequencies of a single stage suspension without PZTs with the resonance frequencies of a dual stage actuated suspension we note that the frequencies of DSA suspensions are reduced as a consequence of the added mass of the PZTs, since

$$f_R = \sqrt{\frac{K}{M}}, \tag{4}$$

where K is the stiffness and M the equivalent mass of the suspension.

Table 2 shows the resonance frequencies for the torsion, bending and sway modes for a typical single stage actuated suspension (SSA) and a typical dual stage actuated suspension (DSA) using the same load beam. For the DSA suspension design we have used the following dimensions: $w_{bridge} = 1.5$ mm, $w_{PZT} = 1.4$ mm, and $w_{edge} = 0.45$ mm. We observe from Table 2, that the bending and torsional frequencies of the single stage suspension are lower than those of the DSA suspension. However, the sway mode of the single stage suspension is higher by approximately 10 % than that of the DSA suspension.

Table 2 Frequencies f_R of SSA and suspension-based DSA

Mode type	Frequency f_R SSA (kHz)	Frequency f_R DSA (kHz)
1st bending	5.59	6.48
2nd bending	10.26	12.23
1st torsion	11.50	11.58
2nd torsion	17.05	17.33
Sway	24.99	21.66

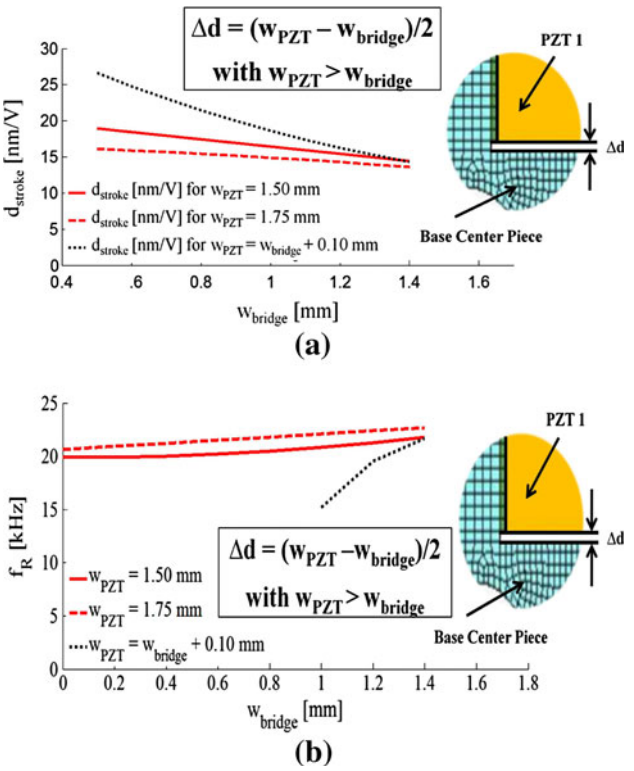

Fig. 4 **a** Stroke d_{stroke} as a function of w_{bridge} at the position of the read–write element and **b** sway mode frequency as a function of w_{bridge}

In the calculations performed in this paper, the hole in the suspension base (see Fig. 1) is neglected.

In Fig. 4a the stroke d_{stroke} is shown at the position of the read–write element as a function of the width of the bridge w_{bridge} for different values of w_{PZT}, the distance between the two PZTs. We note that the stroke decreases with an increase in w_{bridge} and w_{PZT}. On the other hand the sway mode frequency increases (Fig. 4b) for an increase in w_{bridge} and w_{PZT} due to the increase in lateral stiffness.

4 Collocated DSA design

Collocated actuators are defined as actuators in which the PZT is closely aligned with the read–write head to provide improved positioning accuracy of the slider. Jing et al. (2005) investigated a collocated micro-actuator with two

d_{31}-mode piezoelectric elements arranged in a U-shape. A push–pull arrangement similar to suspension-based actuators has also been applied to collocated actuator designs (Koganezawa et al. 2001; Young et al. 2002; Mita et al. 2003).

In addition, collocated actuator designs using the shear (d_{11}, d_{15}) mode have been investigated (Hawwa et al. 2004). Furthermore, Zhu and Wang (2001) proposed a piezoelectric element design with multiple layers of in-plane piezoelectric actuators operating in the bending mode. An alternative with only one d_{31}-mode PZT element was developed by Niu and Fanslau (2004).

In Fig. 5 the design of a flexure-based collocated suspension is shown, consisting of a single piezoelectric microactuator attached to the gimbal structure behind the slider. This design will be investigated in this paper as a representative design for a collocated flexure-based DSA suspension.

As can be seen from Fig. 6, if a voltage is applied to the single PZT attached to the flexure, expansion of the PZT in the x and y direction will occur. Since the mounting pad connections A and B for the PZT on the gimbal are asymmetric with respect to the horizontal centerline of the PZT (see Fig. 6, x-axis), the mounting pad on the right side will be displaced in the positive y-direction by the expansion of the PZT while the pad on the left side will be displaced in the negative y-direction. This, in turn, causes a rotary motion of the flexure arms A and B and, consequently, a rotary motion of the slider attached to the base of the flexure arms.

In Fig. 7 the lay-out of the structure supporting the PZT element is shown. A schematic representation of this lay-out is given in Fig. 8, indicating that it can be idealized as two individual four-bar linkages denoted as 1, 2, 3, 4 and 1′, 2′, 3′, 4′. The following dimensions are of main importance in the design of the collocated DSA shown in Fig. 7:

- the width w_{link} of the upper links 1 and 1′
- the distance l_{link} from the centerline of links 1 and 1′ to the outer edge of the pads to which the PZT is attached

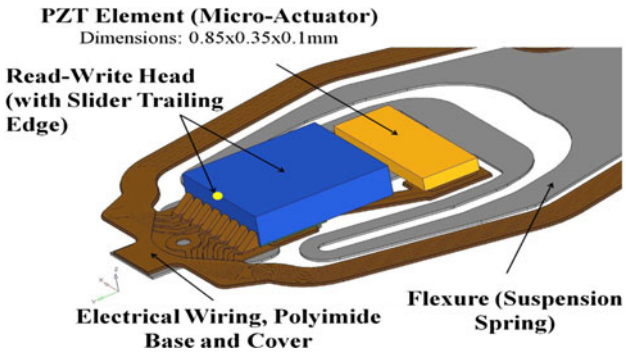

Fig. 5 Collocated flexure-based suspension design

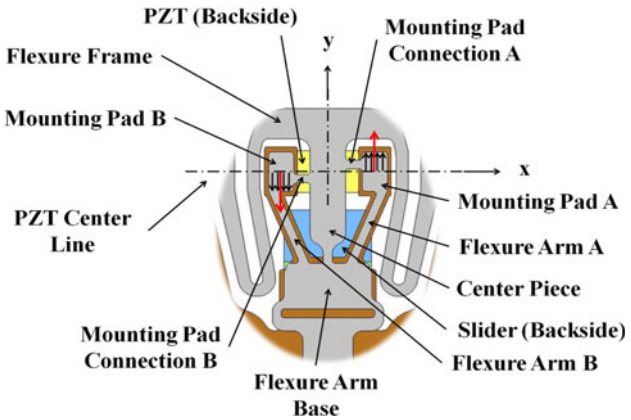

Fig. 6 Operating principle of collocated suspension design

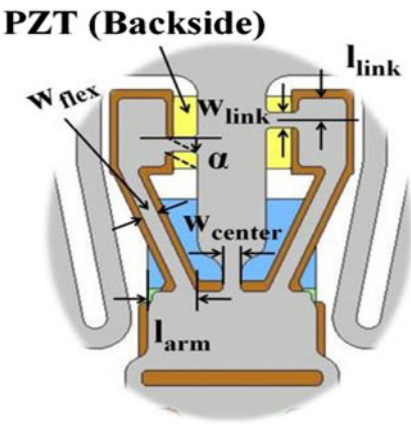

w_{link} (mm)	0.07
l_{link} (mm)	0.09
α (deg)	0
l_{arm} (mm)	0.135
w_{center} (mm)	0.07
w_{flex} (mm)	0.07

Fig. 7 Design parameters of collocated flexure-based DSA with nominal dimensions

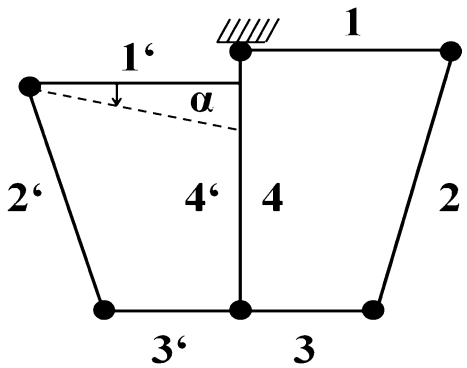

Fig. 8 Idealization of design of DSA as two four-bar linkages

- the distance l_{arm} from the inner side of link 3 and 3′ to the outer edge of the pad for mounting the read–write head
- the width w_{center} of the center link 4 and 4′
- the width w_{flex} of links 2 and 2′.

Numerical calculations are based on the piezoelectric material properties shown in Table 1. All parts of the collocated DSA design were modeled using constant strain solid finite elements with six or eight nodes and three degrees of freedom at each node.

5 Finite element simulation results for collocated DSA suspension

In Fig. 9 the stroke d-$_{stroke}$ is shown for the collocated suspension design of Fig. 7 as a function of the width w_{flex} of links 2 and 2′, respectively. We observe that the stroke decreases with an increase in the width w_{flex} of links 2 and 2′. This result is related to an increase in stiffness with increasing width w_{flex}. Clearly, in order to increase the stroke, the stiffness of the flexure needs to be reduced by decreasing w_{flex}.

Figure 10 shows the stroke d_{stroke} at the read–write element as a function of the distance l_{link}, i.e., the distance

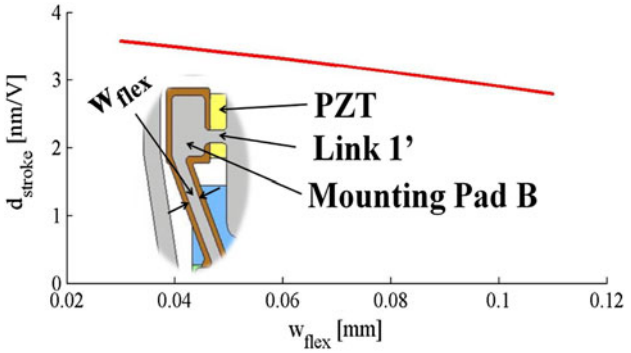

Fig. 9 Stroke d_{stroke} as a function of the width w_{flex} of links 2 and 2′

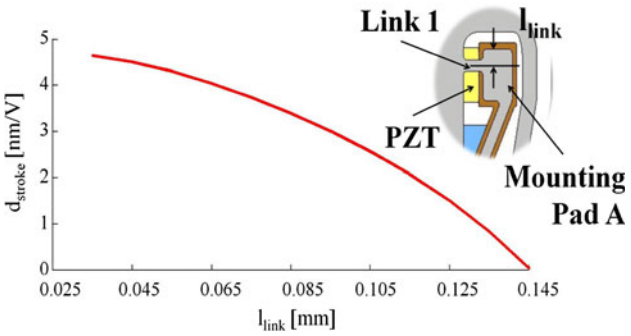

Fig. 10 Stroke d_{stroke} at the position of the read write element as a function of the distance l_{link}

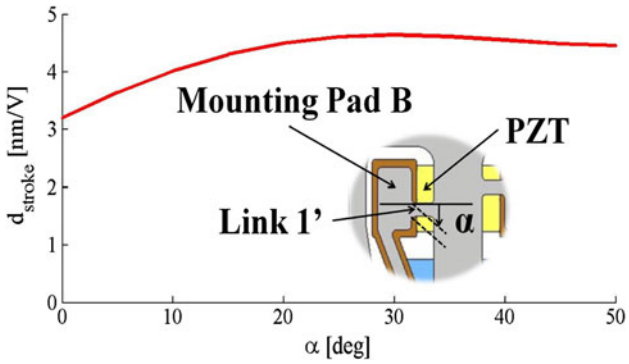

Fig. 11 Lateral deflection d_{stroke} as a function of α

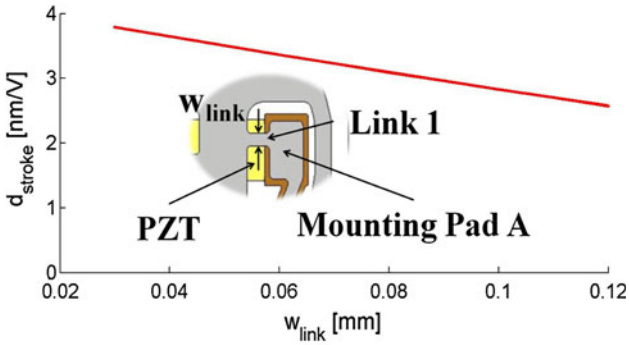

Fig. 12 Stroke d_{stroke} as a function of width w_{link} of links 1 and 1′

from the centerline of link 1 or 1′ to the outer edge of the PZT. We observe that the stroke increases with a decrease of the distance l_{link}. Clearly, the maximum stroke is obtained if the asymmetry of the mounting pad connections is larger, i.e., if the distance between the mounting pad on the right and that on the left is a maximum ($l_{link} \equiv w_{link}/2$).

In Fig. 11 the stroke d_{stroke} is shown as a function of the angle α between links 1 and 4. We observe that d_{stroke} increases with an increase in α, reaching a shallow maximum for α between 30° and 35°.

Figure 12 shows the stroke d_{stroke} as a function of the width of link 1 or 1′, respectively. We observe that d_{stroke} increases as the link width w_{link} decreases. Clearly, this effect is related to the increased flexibility of the four-bar linkages 1, 2, 3, 4 and 1′, 2′, 3′, 4′, respectively, when the in-plane stiffness of links 1 and 1′ is reduced. This result is similar to the result for the change of the stroke as a function of w_{flex} (Fig. 9).

6 Stress distribution of collocated DSA suspension

In Fig. 13 the stress distribution of the collocated DSA investigated in this paper is shown. We observe that the maximum stress σ_{max} occurs at links 1 and 1′. This region is the weakest area of the flexure structure. At this location,

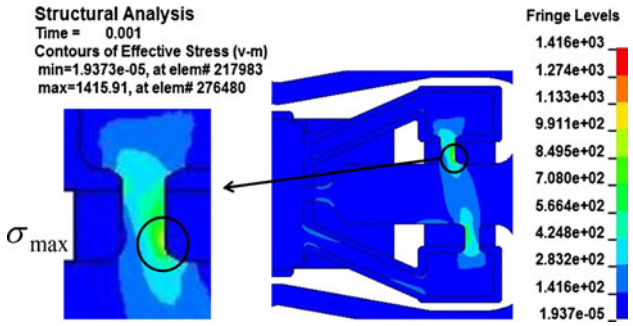

Fig. 13 Maximum stress distributions σ_{max} for flexure of collocated DSA

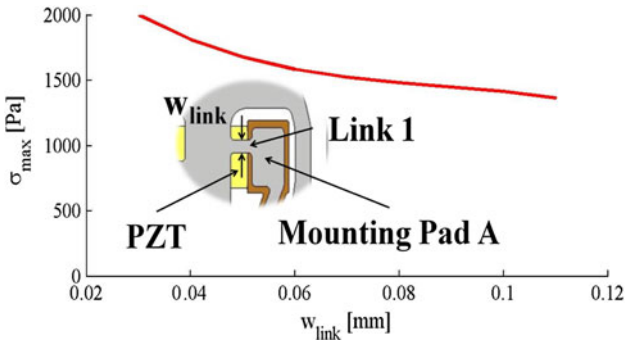

Fig. 14 Maximum stress σ_{max}as a function of the width w_{link} of links 1 or 1′

tensile stress occurs if the PZT expands, while compressive stress occurs if the PZT contracts.

Figure 14 shows the maximum stress σ_{max} as a function of the width of links 1 or 1′. We observe that the maximum stress decreases with an increase in the width w_{link} of links 1 or 1′. In particular, σ_{max} is found to decrease by approximately 30 % if w_{link} is increased from 0.04 to 0.12 mm. Clearly, the value of the maximum stress in the flexure is an important design parameter to be considered in optimizing the stroke of a dual stage suspension.

7 Discussion

The goal of the design of a dual stage suspension is to maximize the stroke for a given voltage input to the PZT. Comparing the numerical results for both designs investigated in this paper, we observe that the suspension-based design provides a much higher stroke. In particular, the typical value of the stroke for a suspension-based design is on the order of 20 nm/V, while the value calculated for the collocated design is typically on the order of 3 to 4 nm/V.

The stroke of a collocated DSA can be optimized beyond the 3–4 nm/V range by changing all important design parameters simultaneously and finding the "global"

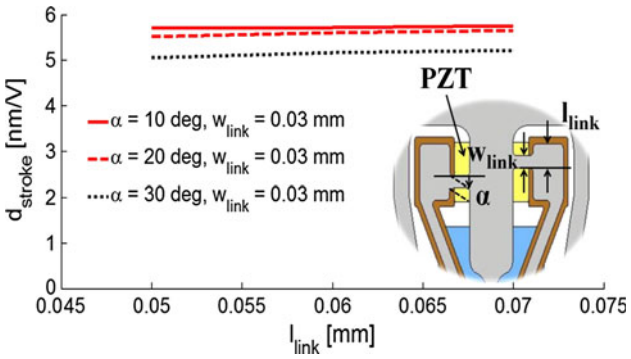

Fig. 15 Stroke d_{stroke} for combinations of l_{link} and α for w_{link} = 0.03 mm of links 1 and 1′

optimum for this design with the constraints that the maximum stress be limited and that the frequency response be adequate.

Optimization methods such as the use of genetic algorithms may be used for finding this global maximum.

A point in support of the statement that a higher stroke is obtained for a careful adjustment of the individual design parameters is shown in Fig. 15 where the stroke d_{stroke} is plotted for a "numerically" optimized combination of design parameters. Here, the stroke d_{stroke} is shown as a function of the distance l_{link} for three values of the link angle α, and w_{link} was chosen to be 0.03 mm.

We observe that the stroke for this design case is on the order of 5–6 nm/V, i.e., substantially larger than the values calculated in Figs. 10, 11 and 12. It should be noted that the largest stroke occurs for a value of α between 10 and 15 degrees.

However, even in this case, we observe that the stroke of the collocated suspension is only about 25–30 % of that of a typical suspension-based design.

In a global optimization of a collocated DSA design, w_{flex} should also be considered as well as w_{link}. In doing this, additional constraints must be introduced on the dimensions of these parameters to guarantee that the maximum stress is not exceeded and that the frequency response is not degraded.

In optimizing the performance of DSA suspensions, additional design parameters affecting the stroke need to be considered. These parameters are the thickness of the adhesion bond (Fig. 16a) and the value of the piezoelectric material constants of the PZT.

With respect to the thickness of the adhesion bond, we see from Fig. 16b that the stroke of the DSA suspension considered decreases as the thickness of the adhesion bond increases keeping all other design parameters including the applied load constant. This behavior is similar for both types of DSA designs. Clearly, a thin bond within close tolerances is desirable to guarantee efficient transmission

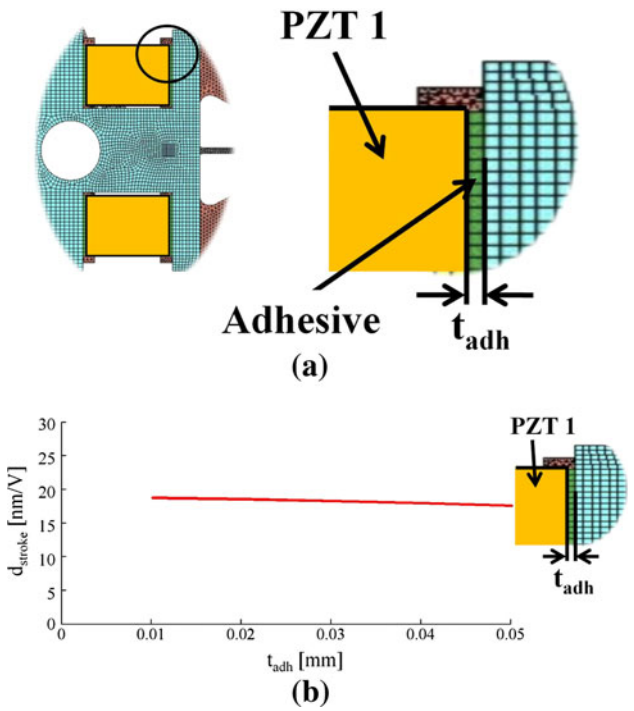

Fig. 16 **a** Design parameter thickness of adhesion bond t_{adh} for suspension-based design and **b** stroke d_{stroke} versus t_{adh}

of shear from the PZT to the flexure but simultaneously ensure adequate attachment.

The other parameter of importance in obtaining a large stroke is the value of the piezoelectric expansion coefficient of the PZT. Clearly, the material used should have the highest values possible. Since the effect of the material properties is linear with respect to the stroke, the same linear change in stroke will be observed for either design.

8 Conclusions

In this investigation a typical suspension-based and collocated dual stage suspension was investigated. The following conclusions can be drawn for the suspension-based DSA design:

1. The lateral displacement of suspension-based DSAs is inversely proportional to w_{PZT}, the distance between the PZTs. That is, the smaller w_{PZT} the higher is the stroke.
2. The stiffness of the suspension increases with an increase in w_{bridge} which, in turn, increases the sway mode frequency but reduces the stroke (Fig. 4).
3. For the collocated flexure-based dual stage suspension design we observe that:
4. The achievable stroke is on the order of one fourth of the stroke of a typical suspension-based design for similar voltage levels.
5. The asymmetry of the positioning of links 1 and 1′ should be as large as possible ($l_{link} = w_{link}/2$) in order to maximize the stroke of the suspension
6. The stroke of the collocated suspension increases with a decrease in w_{link} and w_{flex}. This, however, degrades the frequency response.
7. To achieve maximum stroke it is necessary to optimize all design parameters simultaneously, i.e., w_{link}, l_{link} of links 1 and 1′ and α between links 1 and 4 and 1′ and 4.

For both suspension types the thickness of the adhesion bond should be as thin as practical to achieve highest stroke. Also, the material properties of the PZT should be chosen to correspond to largest expansion values possible.

In all cases a trade-off exists between providing the highest stroke, desirable resonance frequency characteristics and minimum stresses.

Acknowledgments We would like to thank Hanya-san and John Hogan of NHK for their interest and support of this study.

References

Devasia S, Eleftheriou E, Moheimani SOR (2007) A survey of control issues in nanopositioning. IEEE Trans Control Syst Technol 15(5):802–823

Evans RB, Griesbach JS (1999) Piezoelectric microactuator for dual stage control. IEEE Trans Magn 35(2):977–982

Hawwa MA, Fanslau EB, Young KF (2004) Shear mode multilayered collocated micro-actuator for dual-stage servo controllers in disk drives. United States Patent US 6,704,158 B2

Jing Y, Luo J, Huang P, Qin L (2005) U-type piezoelectric thin-film microactuator for hard disk drives. IEEE Trans Magn 41(11):4309–4314

Kilian S, Zander U, Talke FE (2003) Suspension modeling and optimization using finite element analysis. Tribol Int 36:317–324

Kim YH, Lee SH (2004) An approach to dual-stage servo design in computer disk drives. IEEE Trans Control Syst Technol 12(1): 12–20

Koganezawa S, Uematsu Y, Yamada T, Nakano H, Inoue J, Suzuki T (1998) Shear mode piezoelectric microactuator for magnetic disk drives. IEEE Trans Magn 34(4):1910–1912

Koganezawa S, Kohei T, Yamada T, Uematsu Y, Noguchi T, Nakano H, Sakamoto R, Inoue J, Suzuki T (2001) Actuator using piezoelectric element and head-positioning mechanism using the actuator. United States Patent US 6,327,120 B1

Lau GK, Du H (2005) A piezoelectric micro-actuator with extended base-plate for HDD. Microsyst Technol 11:598–605

Lau GK, Du H (2006) A piezoelectric quad-morph actuated suspension for hard disk drives. J Mircomech Mircroeng 16:1833–1840. doi:10.1088/0960-1317/16/9/011

Mita T, Hida M, Kurihara K (2003) Piezoelectric actuator set for head assembly. United States Patent US 6,617,763 B2

Mori K, Munemoto T, Otsuki H, Yamaguchi Y (1991) A dual stage magnetic disk drive actuator using a piezoelectric device for a high track density. IEEE Trans Magn 27(6):5298–5300

Niu Y, Fanslau Jr EB (2004) Microactuator with offsetting hinges and method for high-resolution positioning of magnetic read/write head. United States Patent US 6,760,196 B1

Young KF, Fanslau EB, Hawwa MA (2002) Collocated rotating flexure microactuator for dual-stage servo in disk drives. United States Patent US 6,376,964 B1

Zhong ZW, Sun J (2004) A suspension integrated with a piezoelectric microactuator for dual stage actuation. Int J Adv Manuf Technol 24:686–692

Zhu W, Wang Z (2001) A multilayer inplane bending piezoelectric actuator for dual-stage head-positioning control system. J Mater Sci 12:111–116